Direct *In Situ* Measurement of an Ultrashort Pulse Using an Optical Hologram

Huiyao Xu,[1] Wei Cao,[1,*] Kang Mi,[1] Yunlong Mo,[1] Xi Chen,[1] Qingbin Zhang,[1] and Peixiang Lu[1,2,†]

[1]*School of Physics and Wuhan National Laboratory for Optoelectronics, Huazhong University of Science and Technology, Wuhan 430074, China*

[2]*Optics Valley Laboratory, Wuhan 430074, China*

The dipole response of helium exposed to attosecond extreme ultraviolet (EUV) pulses and a femtosecond near-infrared (NIR) laser field is investigated. The optical interference between the EUV pulse and nonlinear wave-mixing signals leads to fringes in the transmitted spectrum above the single ionization threshold. Perturbation theory suggests that such fringes record the self-convolution of complex-valued NIR pulse in the frequency domain, allowing direct characterization of a broadband optical pulse without the need of reconstruction algorithms. We apply this *in situ* interferometric scheme to diagnose a few-cycle laser pulse.

I. INTRODUCTION

Broadband femtosecond pulses are of particular relevance due to their wide applications in quantum state manipulation in atomic systems [1,2], coherent control of photochemical reaction [3–5], and light-induced phase transition in condensed matter [6–8]. The prior knowledge of the amplitude and phase information of the pulses is generally a prerequisite for triggering light-matter interaction that follows the desired reaction pathways [9,10]. The most commonly used method for complete characterization of a laser pulse is the frequency-resolved optical gating (FROG) [11]. In order to recover the phase information that is missing in the measured spectrogram, a phase-retrieval algorithm is used repeatedly and will normally converge to the correct solution of the pulse. Recently, Keiber *et al.* [12] has extended the electro-optic sampling method to the near-infrared (NIR) region. The waveform of the NIR pulse can be well characterized without using a complex data-retrieving algorithm. Other methods such as spectral phase interferometry for direct electric field reconstruction (SPIDER) [13,14], dispersion scan (d-scan) [15], and two-dimensional spectral-shearing interferometry (2DSI) [16] are also developed and provides reliable alternative pulse diagnosing schemes that are performed under ambient environment. However, these mentioned methods pose potential limitations, that is they rely on nonlinear processes inside the crystal and the dispersion inside the nonlinear crystal is inevitably introduced, which could

cause remarkable deviation for pulses with bandwidths of several hundred nanometers.

To avoid the mentioned issues, direct measurement of an optical pulse in a nondispersive environment is also performed using high-order harmonic based attosecond pulses. Goulielmakis *et al.* demonstrated the oscilloscope for optical pulses using an attosecond streak camera, in which the center of mass of the photoelectron spectrum directly maps out the vector potential of the electric field of an optical pulse [17]. Such photoelectron spectroscopy, however, is bandwidth limited due to the central momentum approximation, and is also time consuming in order to avoid the space-charge effect. Several all-optical approaches based on laser-driven high harmonic generation (HHG) have also shown their capabilities for successful reconstruction of the waveform of an optical pulse [18–21]. These strong field-based schemes could produce plasma that can distort the waveform of the electric field to be diagnosed, which can be detrimental for further applications. Recently, we demonstrated an all-optical attosecond waveform-sampling scheme for an optical pulse with extreme ultraviolet (EUV) absorption spectroscopy [22]. Moderately intense nonionizing lasers are utilized. A three-pulse configuration (one attosecond EUV pulse and two NIR pulses) is adopted to induce ac Stark effect in helium atoms. And the quasienergies of the laser-dressed atom reflect the time-domain waveform of an optical pulse with attosecond accuracy. Such absorption spectroscopy minimizes the plasma-induced pulse distortion and provides an effective approach for optical pulse measurement.

In this work, we further explore the potential capability for pulse measurement of EUV transient

*weicao@hust.edu.cn

†lupeixiang@mail.hust.edu.cn

absorption spectroscopy. Instead of tuning the quasienergies of the laser-dressed atom by delaying the two NIR pulses in the previous scheme [22], we use only one NIR pulse and inspect the interference hologram in the absorption spectrum above the first ionization threshold of helium. Both perturbative analysis and numerical simulation indicate that such a hologram is caused by optical interference between the EUV pulse and the nonlinear wave-mixing signals. By performing windowed Fourier-transform wave-mixing, the signal mediated by a single excited state can be filtered out, such filtered fringes record the self-convolution of the complex-valued NIR pulse in the frequency domain, allowing the NIR pulse to be directly characterized. We utilize the current method to successfully measure a NIR pulse spanning from 600 to 900 nm. As compared to the previous one, the current method needs only two pulses and greatly improves the feasibility and ease of use.

II. PRINCIPLE

To explain this *in situ* interferometric scheme, we consider an atomic system interacting with the EUV and NIR pulses. Starting from the ground state, the atom is promptly excited by the attosecond pulse and a wavepacket: $\psi(t,r) = \sum_m C_m(t)\varphi_m(r)e^{-iE_m t}$ is prepared, where $C_m(t)$, E_m stand for the amplitude and energy of eigenstate $|m\rangle$, respectively. The NIR pulse then couples the excited states and perturbs the evolution of the initiated wavepacket. Considering a nonresonant moderately intense NIR laser pulse, the second-order perturbation theory (SOPT) [23] can be applied to depict the time-dependent amplitude of excited state $|n\rangle$:

$$\Delta C_n(t,\tau) = -\int_0^t \varepsilon(t',\tau)\sum_k d_{nk}e^{-i\Delta_{kn}t'}dt'$$
$$\times \int_0^{t'} \varepsilon(t'',\tau)\sum_m C_m(t'')d_{km}e^{i\Delta_{km}t''}dt'', \quad (1)$$

where ε represents an arbitrary electric field. d_{nk} is the dipole-matrix element between excited states $|n\rangle$ and $|k\rangle$. $\Delta_{ij} = E_i - E_j$ is the transition energies. The delay-dependent optical density of the relevant channel that is responsible for the absorption of two NIR photons, can be expressed as (more details can be found in Sec. S1 within the Supplemental Material [24,25]):

$$OD_n^\Omega(\Omega + \Delta_{mn}, \tau)$$
$$\propto \text{Im}\left\{\sum_n \Delta C_n^\Omega(\Omega + \Delta_{mn}, \tau)d_{gn}\right\}$$

$$\propto \text{Re}\left\{e^{i\Omega\tau}\int d\omega A_\omega A_{\Omega-\omega}e^{-i(\varphi_\omega + \varphi_{\Omega-\omega})}\right.$$
$$\left.\times \sum_m \sum_k \frac{d_{gm}d_{nk}d_{km}}{-(\Omega - \omega - \Delta_{km})(\Omega + \Delta_{mn})}\right\}, \quad (2)$$

where ω is the frequency of the NIR pulse. Ω is the sum frequency of the two NIR photons. A_ω and φ_ω are the spectral amplitude and spectral phase of the NIR pulse. Here, $OD_n^\Omega(\Omega + \Delta_{mn}, \tau)$ represents the optical density at the energy $E_n + \Omega + \Delta_{mn}$ for a particular delay τ between the EUV and NIR laser fields. Equation (2) summarizes all the channels that contribute to the rapid modulation with a period of $2\omega_0$ along the delay axis in the absorption spectrogram, ω_0 stands for the central frequency of the NIR pulse. For the special case $\Delta_{mn} = -\Omega$, it corresponds to a ladder-type resonant two-photon transition between states $|n\rangle$ and $|m\rangle$, where pronounced population transfer occurs [26]. When both $|\Delta_{mn}|$ and $|\Delta_{km}|$ are much smaller than Ω, such as excited states close to the ionization threshold, the prefactor $\sum_m \sum_k \frac{d_{gm}d_{nk}d_{km}}{-(\Omega - \omega - \Delta_{km})(\Omega + \Delta_{mn})}$, which describes the two-photon transition amplitude, becomes insensitive to frequency ω, and Eq. (2) can be further simplified as

$$OD_n^\Omega(\Omega + \Delta_{mn}, \tau)$$
$$\propto \text{Re}\left\{e^{i\Omega\tau}\sum_m \sum_k \frac{d_{gm}d_{nk}d_{km}}{-(\omega_0 - \Delta_{km})(2\omega_0 + \Delta_{mn})}\right.$$
$$\left.\times \int d\omega A_\omega A_{\Omega-\omega}e^{-i(\varphi_\omega + \varphi_{\Omega-\omega})}\right\}. \quad (3)$$

Here it is legitimate to use the constant $\sum_m \sum_k \frac{d_{gm}d_{nk}d_{km}}{-(\omega_0 - \Delta_{km})(2\omega_0 + \Delta_{mn})}$ to represent the two-photon transition amplitude. Equation (3) is the main analytical formula for pulse characterization in this work. $\int d\omega A_\omega A_{\Omega-\omega}e^{-i(\varphi_\omega + \varphi_{\Omega-\omega})}$ is the self-convolution of the NIR pulse in the frequency domain. It is then straightforward to retrieve the waveform of the time-domain electric field using the convolution theorem.

In order to verify the correctness of this method, we carry out numerical simulations based on a multilevel model [27]. The ground state $1s^2$, excited state $1s4p$ (23.77 eV), and dark state $1s4s$ (23.67 eV) of a helium atom are considered in the simulation. The 800-nm NIR pulse has a transform-limited pulse duration of 7 fs, and a peak intensity of 8×10^{11} W/cm^2. For generality, we propagate the NIR pulse through 1-mm fused silica (FS) to include a certain amount of dispersion. The EUV attosecond pulse has a duration of 250 as and a central frequency of 25 eV, the peak intensity is 1×10^{10} W/cm^2. The delay-dependent absorption spectrum is shown in Fig. 1(a). The absorption features appearing around zero delay (22 and 25 eV)
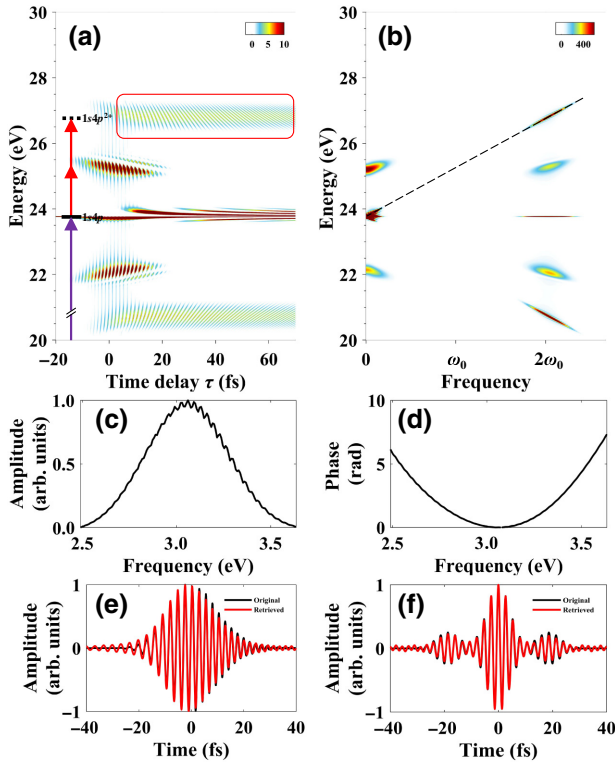
FIG. 1. Principle of *in situ* measurement of ultrashort laser pulse using optical hologram. (a) Simulation results of the transient absorption spectroscopy in helium using a multilevel model. (b) Two-dimensional spectrograms obtained from (a) by Fourier transformation along the time-delay axis (the NIR central frequency $\omega_0 = 1.55$ eV). The dashed black lines indicate the 2ω oscillation of the interference fringes associated with the $1s4p$ intermediate state. (c),(d) Amplitude and phase of the interference fringes in the frequency domain, respectively. (e),(f) The retrieved (red solid lines) as compared with the original (black solid lines) electric fields of the NIR pulses. (e) A Gaussian temporal envelope with 1-mm fused-silica dispersion and (f) a complex temporal envelope.

correspond to light-induced states (LISs). The tilt of these features is due to the frequency sweep of the NIR pulse and can be used to probe the time-dependent quasienergy of laser-dressed state [28]. We also see the quantum-interference fringes that is two NIR photons away from the excited state $1s4p$. The $1s4p$ state is initially populated by the EUV pulse, then the NIR pulse modulates the amplitude of $1s4p$ and populates a virtual quantum state $1s4p^{2+}$, the radiated dipole is induced (the nonlinear wave-mixing signal) by the coherence between the $1s^2$ and $1s4p^{2+}$ states. This dipole carries frequency in the EUV regime and can interfere with the incidental EUV field forming interference fringes in the absorption spectrum. This is the main structure that is responsible for Eq. (3) and can be utilized for pulse characterization.

The pulse-retrieval procedure follows three steps. First, Fourier transform of the delay-dependent optical density is performed along the time-delay axis providing the two-dimensional spectrogram, as shown in Fig. 1(b). The features with 2ω oscillation along the delay axis lie on the slope 1 line [indicated by the black dashed line in Fig. 1(b)] in the Fourier spectrogram and correspond to the absorption of two NIR photons [29], and the intercept point of the black dashed line with the energy axis corresponds to the energy of the intermediate bright state. Second, integrating the 2ω oscillations along the frequency axis (horizontal axis) gives a complex-valued spectrum (note that the energy axis has been shifted downward by the intrinsic energy of $1s4p$). The amplitude and phase of this spectrum are shown in Fig. 1(c) and Fig. 1(d), respectively. In particular, due to the limited time window used for the Fourier transform, a relatively small spectral modulation appears in Fig. 1(c). Following Eq. (3), this integrated spectrum is proportional to the self-convolution function of the NIR field. Third, according to the convolution theorem, the self-convolution function of the NIR pulse in the frequency domain is equal to the Fourier transform of the square of the time-domain waveform $E(t)$: $E(t)^2 \propto \int \left(\int d\omega A_\omega A_{\Omega-\omega} e^{-i(\varphi_\omega + \varphi_{\Omega-\omega})} \right) e^{i\Omega t} d\Omega$, from which $E(t)$ can be directly retrieved. The retrieved results are shown in Fig. 1(e). The black line in Fig. 1(e) is the waveform of the original NIR pulse, and the red line is the retrieved one. The retrieved electric field is in good agreement with the original one, the small oscillations on the baseline are artifact due to the limited window of the Fourier transform. We also testify the reconstruction of a pulse with more complex temporal structure and the results are shown in Fig. 1(f). The good agreement between the input and retrieved pulse indicates the validity of the current method.

It should be noted that the above numerical simulations consider only the three-photon transition (i.e., one EUV photon and two NIR photons) via a single intermediate bright state (i.e., $1s4p$ state). For a real atom, multiple excited states converging to the ionization threshold can contribute to the final interference pattern. Figure 2(a) shows the attosecond transient absorption of a model atom by numerically solving the time-dependent Schrödinger equation. The parameters for the NIR and EUV attosecond pulses are the same as in Fig. 1 except that the central frequency of the NIR pulse is slightly higher ($\omega_0 = 2$ eV) to match the same energy of the final state (approximately 27 eV). Other than the virtual states and stark effect of each bright state below an ionization threshold of 24 eV, absorption of two NIR photons from the Rydberg states contributes to the interference fringes around 27 eV, which are relevant to the hologram that we are interested in for pulse retrieval. Fourier transform of the absorption spectrum along the time-delay axis provides the two-dimensional spectrogram, as shown in Fig. 2(b). From Fig. 2(b), we can see that multiple excited states
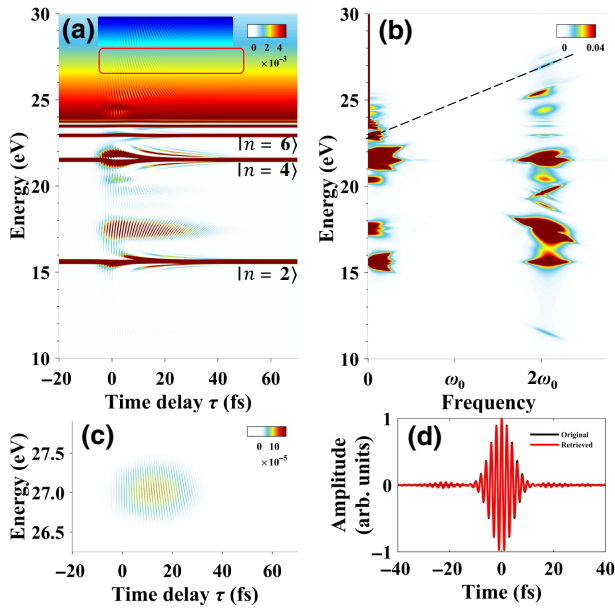
FIG. 2.　Simulation and reconstruction results. (a) Transient absorption spectroscopy of a model atom by numerically solving the time-dependent Schrödinger equation (inset emphasizes the interference fringes indicated by the red box using a different color bar). (b) Two-dimensional spectrograms obtained from (a) by Fourier transformation along the time-delay axis (the NIR central frequency $\omega_0 = 2$ eV). The dashed black lines indicate the 2ω oscillation of the interference fringes associated with transition via the third excited bright state $|n = 6\rangle$. (c) The interference spectrum obtained by windowed inverse Fourier transform along the dashed black line in (b). (d) Retrieved results of the temporal profile of femtosecond pulse from (c). The black line is the waveform of the original pulse, the red line is the retrieved waveforms.

converging to the ionization threshold contribute to the final interference pattern associated with absorption of two NIR photons indicated by the red box. If multiple pathways are selected for analysis, there will be quantum beat effects [30–32] in the final interference pattern, which is detrimental to direct pulse reconstruction. Therefore, it is necessary to filter out the transition involving a single intermediate excited state for analysis. Here, we choose the $|n = 6\rangle$ intermediate state to retrieve the signal pulse waveform. This is implemented by filtering out the frequency components along the black dashed line in Fig. 2(b), and the filtered interference fringes are shown in Fig. 2(c). The retrieved results are shown in Fig. 2(d). It shows that even multiple excited states may complicate the interference patterns, the method is still applicable through frequency-domain filtering. (See Fig. S1 and Fig. S2 within the Supplemental Material for the successful retrieval of more complex waveforms [24].) Therefore, we verify the correctness of the method from the multilevel model and the feasibility of the method from the time-dependent

Schrödinger equation. Next, we apply this method to experimentally measure the NIR-pulse waveforms.

III. EXPERIMENTAL SETUP

The experimental setup is shown in Fig. 3(a), which is similar to the one in Ref. [28]. A 1-mJ 800-nm Ti:sapphire laser pulse with a duration of 25 fs is focused into a neon-filled hollow core fiber for spectral broadening (600–900 nm), followed by chirp mirrors for dispersion compensation. Then a 7-fs few-cycle NIR laser pulse is obtained. The NIR laser pulse is focused into a 15-torr xenon gas
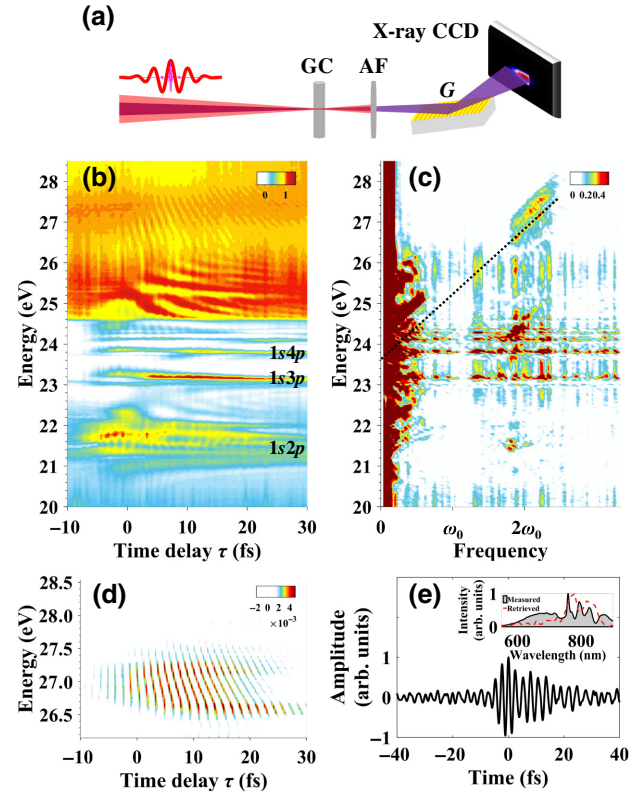

FIG. 3.　Experimental measurement of ultrashort laser pulse using optical hologram. (a) Schematic of the experimental setup. GC, gas cell for transient absorption; AF, aluminum filter; *G*, grating. (b) The experimentally measured optical density (OD) of singly excited states (SES) in a helium atom, as a function of time delay between the NIR and EUV laser pulse. The peak intensity of the NIR pulse is approximately $1 \times 10^{12} \text{W/cm}^2$ and is carefully compressed; the delay step is 400 as. Negative delay means the NIR pulse precedes the EUV pulse. (c) Two-dimensional spectrogram obtained from the data shown in (b) by Fourier transformation along the time-delay axis (the NIR central frequency $\omega_0 = 1.55$ eV). The dashed black lines indicate the 2ω oscillation of the interference fringes associated with the $1s4p$ intermediate state. (d) Interference spectrum obtained by windowed inverse Fourier transform along the dashed black line in (c). (e) Waveform retrieved from (d). Inset shows the measured (filled gray line) and retrieved spectrum (dashed red curve) of the NIR pule.

for HHG, resulting in EUV attosecond bursts that have a pulse duration of about 400 as around 21 eV. The NIR laser pulse and the EUV laser pulse are collinearly propagating and focused on a second gas cell filled with helium gas. In order to block the NIR laser pulse from reaching the x-ray CCD camera, a 200-nm aluminum filter is inserted downstream of the interaction gas to block the transmitted NIR laser pulse. The transmitted spectrum of the EUV beam is diagnosed by an EUV spectrometer with a resolution of 25 meV, which consists of a flat-field grating and a x-ray CCD camera. The relative delay between the NIR and EUV laser pulse is precisely controlled by a piezoelectric transducer. In order to control the waveform of the femtosecond laser pulse, we add FS with variable thicknesses in the NIR light path to introduce different amounts of dispersion (more details can be found in Sec. S5 within the Supplemental Material [24]).

IV. RESULTS AND DISCUSSION

The experimental results are shown in Fig. 3. Figure 3(b) is the transient absorption spectrum around the first ionization threshold in the helium atom, which shows a rather similar pattern to the simulated results in Fig. 2(a). In Fig. 3(b), we can see that for large negative delays ($\tau \approx$-10 fs), because the NIR and EUV laser pulse are well separated in time, clear absorption lines primarily due to the EUV-induced single-photon transition are observed in the spectrum. Near the zero delay ($-5 < \tau < 10$ fs), where the NIR and EUV overlap temporally, more absorption features emerge. Such as Autler-Townes (AT) splitting ($1s2p$ state), ac Stark shift (> 23 eV), and light-induced states (22, 25 eV) [33–37]. For large positive delays ($\tau > 20$ fs), the EUV pulse is preceding the NIR pulse. The EUV-induced free induction decay (FID) [38], can be perturbed by the delayed NIR pulse, leading to hyperbolic lines in the absorption spectrum. These features have been studied extensively in ATAS experiments to uncover the ultrafast dynamic information in helium atoms [35–37,39–41]. The interference structure about 3 eV above the ionization threshold (around 27 eV) is less explored and is a detectable quantity that can be utilized for pulse reconstruction as demonstrated in the principle section.

The Fourier analysis of the transient absorption spectrogram [as shown in Fig. 3(c)] indicates that the interference around 27 eV has a modulation period of about 1.3 fs (the corresponding frequency is 3.1 eV). These features consist of multiple components that lie on slope 1 lines, indicating several $1snp$ excited states converging to the ionization threshold of helium are involved. These experimental observations are in line with the simulation results [see Fig. 2(b)], except that these features in the Fourier domain are not well separated along the energy axis as compared to Fig. 2(b). This is due to limited resolution

of the EUV spectrometer used in our experiment. However, we can still filter out the lowest $1s4p$ channel as indicated by the black dashed line in Fig. 3(c). The filtered OD spectrum around 27 eV is shown in Fig. 3(d). The interference pattern clearly shows a more complicated structure than Fig. 2(c) in which the NIR pulse contains mainly the second-order dispersion. This indicates that higher-order dispersion exists in the experimentally used NIR pulse. The retrieved electric field of the NIR pulse is shown in Fig. 3(e). Although the NIR pulse is carefully compressed to a close to Fourier-limited one, the pulse does contain higher-order dispersion, even if it is relatively small. The inset of Fig. 3(e) provides the comparison between the measured (filled, gray line) and retrieved spectrum (dashed red curve) of the NIR pulse. They show good consistency. Through fitting, the FWHM of the NIR laser pulse is about 7 fs.

In order to experimentally verify the measurement of arbitrary pulses, we add FS with variable thicknesses in the NIR light path to control the waveform of the femtosecond laser pulse [42]. The retrieved results are shown in Fig. 4(a). The black line in Fig. 4(a) is the simulated electric field assuming the pulse is overcompensated by 0.5-mm FS as compared to the one retrieved in Fig. 3(e), and the red line is the directly measured waveform after inserting an extra 0.5-mm FS in the experiment. It can be seen that the retrieved result is in good agreement with the simulated one. Figure 4(b) compares the measured (red line) and calculated (black line) spectral phase change induced by 0.5-mm FS. The bending of the phase curve is primarily contributed from second-order dispersion. The retrieved group-delay dispersion (GDD) introduced by the fused silica is 21.07 fs^2 as compared to the predicted value of 22.47 fs^2 at the wavelength of 700 nm. The overall good agreement between the predicted and measured spectral phase demonstrates the reliability of the current method for measuring pulses with higher-order dispersions. Here,
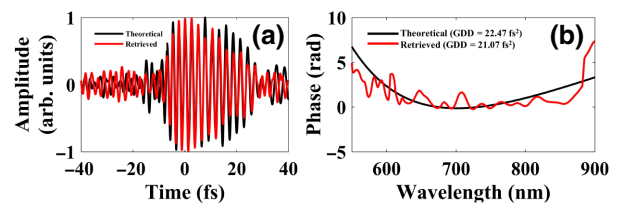

FIG. 4. Measurement of ultrashort laser pulse with higher-order dispersions. (a) The retrieved results of the temporal profile of femtosecond pulse with positive dispersions, the red line is the experimentally retrieved result and the black line is the calculated electric field from the result in Fig. 3(e) by adding dispersion of 0.5-mm FS. (b) Phase information of the femtosecond pulse in the frequency domain, the red line is the retrieved result and the black line is the predicted result. The theoretical GDD is 22.47 fs^2 at the wavelength of 700 nm, and the retrieved GDD is 21.07 fs^2.

it should be noted that the single attosecond pulse is used in the numerical simulations, in the experiment, the generated EUV pulse is not a single attosecond pulse but an attosecond pulse train (APT) containing a few attosecond bursts separated by half an optical cycle of the driving field. Because the NIR pulse to be measured is a replica of the NIR pulse that is used for EUV pulse generation, each attosecond pulse is precisely phase locked to the carrier of the NIR field according to the mechanism of high harmonic generation [43,44]. We perform numerical simulations using an attosecond-pulse train as the pump, and the calculations show that the use of an attosecond-pulse train instead of a single attosecond pulse can still correctly recover the waveform of the NIR pulse (more details can be found in Sec. S3 within the Supplemental Material [24]).

We also experimentally investigated the influence of the NIR pulse under different polarization directions with respect to that of the EUV pulse. We introduce a half-wave plate in the arm of the NIR beam to control the polarization state of the NIR pulse. The experimental results indicate that the direction of the NIR polarization does not affect the retrieved waveform of the NIR pulse (see Sec. S5 within the Supplemental Material [24]). However, the modulation depth of the interference fringes is larger for parallel configuration (polarization direction of EUV and NIR are parallel to each other) as compared to the perpendicular one (polarization direction of EUV and NIR are perpendicular to each other). Such a polarization dependence can be qualitatively explained using the second-order perturbation theory. Assuming the EUV polarization is along the quantum axis z, under the single active electron approximation [40], the transition amplitude from the EUV excited p orbital to the final orbital can be estimated with the spherical harmonic basis $|Y_l^m\rangle$: $P \propto \sum_{l,m} \langle Y_l^m |d_{\mathrm{NIR}}| Y_1^{\,0}\rangle \times$

$\langle Y_{l'}^{m'} |d_{\mathrm{NIR}}| Y_l^m\rangle$, where d_{NIR} is the dipole operator. For parallel configuration, $d_{\mathrm{NIR}} \propto Y_1^0$, for perpendicular configuration, $d_{\mathrm{NIR}} \propto \left(1/\sqrt{2}\right)\left(Y_1^{-1} - Y_1^1\right)$. And the calculated ratio of the transition amplitude between parallel and perpendicular configuration is $P_\parallel : P_\perp = 3 : 1$ (see Sec. S4 within the Supplemental Material [24]). The predicted ratio is consistent with the measurement. Therefore, the correct retrieval of the electric field is not sensitive to the polarization of the NIR field as long as it is linearly polarized.

V. CONCLUSIONS

In summary, this work provides a method to retrieve the waveforms of optical pulses, using attosecond transient absorption spectroscopy. In a pulse sequence where the attosecond EUV pulse precedes the NIR field, the wave-mixing nonlinear signals show interference fringes due to optical quantum interference. Perturbation theory including a few essential quantum levels indicates that the frequency-domain expression of interference fringes is equivalent to the self-convolution of the complex-valued NIR pulse, from which the electric field of the NIR pulse can be directly characterized. For a real atomic system that contains many excited states, the NIR pulse can still be well characterized through frequency-domain filtering. We experimentally demonstrate the successful retrieval of a few-cycle NIR pulse. We also discuss the influence of the direction of the NIR-pulse polarization on the retrieved results. Both theoretical analysis and experimental results show that the polarization direction of the electric field does not affect the retrieved results. This method has a simple principle, and provides a means for retrieving the linearly polarized NIR pulse with arbitrary waveforms. It is worth noting that the response frequency of this method is not limited to ultrashort pulses with a center wavelength of 800 nm. It is expected that it can be extended to the measurement of ultrashort pulses in ultraviolet or with even shorter wavelengths in the future.

[1] S. Gilbertson, M. Chini, X. Feng, S. Khan, Y. Wu, and Z. Chang, Monitoring and Controlling the Electron Dynamics in Helium with Isolated Attosecond Pulses, Phys. Rev. Lett. **105**, 263003 (2010).

[2] C. Ott, A. Kaldun, L. Argenti, P. Raith, K. Meyer, M. Laux, Y. Zhang, A. Blättermann, S. Hagstotz, T. Ding, R. Heck, J. Madroñero, F. Martín, and T. Pfeifer, Reconstruction and control of a time-dependent two-electron wave packet, Nature **516**, 374 (2014).

[3] R. de Vivie-Riedle, L. Kurtz, and A. Hofmann, Coherent control for ultrafast photochemical reactions, Pure Appl. Chem. **73**, 525 (2001).

[4] B. J. Sussman, D. Townsend, M. Y. Ivanov, and A. Stolow, Dynamic Stark control of photochemical processes, Science **314**, 278 (2006).

[5] G. Cerullo and C. Vozzi, Coherent control of chemical reactions on the attosecond time scale, Physics **5**, 138 (2012).

[6] N. F. Brady, K. Appavoo, M. Seo, J. Nag, R. P. Prasankumar, R. F. Haglund Jr, and D. J. Hilton, Heterogeneous nucleation and growth dynamics in the light-induced phase transition in vanadium dioxide, J. Physics: Condens. Matter **28**, 125603 (2016).

[7] D. Afanasiev, B. Ivanov, R. Pisarev, A. Kirilyuk, T. Rasing, and A. Kimel, Femtosecond single-shot imaging and control of a laser-induced firstorder phase transition in hofeo3, J. Physics: Condens. Matter **29**, 224003 (2017).

[8] A. Zong, A. Kogar, Y.-Q. Bie, T. Rohwer, C. Lee, E. Baldini, E. Ergeçen, M. B. Yilmaz, B. Freelon, E. J. Sie, H. Zhou, J. Straquadine, P. Walmsley, P. E. Dolgirev, A. V. Rozhkov, I. R. Fisher, P. Jarillo-Herrero, B. V. Fine, and N. Gedik, Evidence for topological defects in a photoinduced phase transition, Nat. Phys. **15**, 27 (2019).

[9] A. Korobenko, K. Johnston, M. Kubullek, L. Arissian, Z. Dube, T. Wang, M. Kübel, A. Y. Naumov, D. Villeneuve, M. F. Kling, P. B. Corkum, A. Staudte, and B. Bergues, Femtosecond streaking in ambient air, Optica **7**, 1372 (2020).

[10] D. Zimin, M. Weidman, J. Schötz, M. F. Kling, V. S. Yakovlev, F. Krausz, and N. Karpowicz, Petahertz-scale nonlinear photoconductive sampling in air, Optica **8**, 586 (2021).

[11] D. J. Kane and R. Trebino, Characterization of arbitrary femtosecond pulses using frequency-resolved optical gating, IEEE J. Quantum Electron. **29**, 571 (1993).

[12] K. Sabine, S. Shawn, S. Alexander, T. Michael, P. Volodymyr, K. Ferenc, and K. Nicholas, Electro-optic sampling of near-infrared waveforms, Nat. Photonics **10**, 159 (2016).

[13] C. Iaconis and I. A. Walmsley, Spectral phase interferometry for direct electric-field reconstruction of ultrashort optical pulses, Opt. Lett. **23**, 792 (1998).

[14] B. Peter and R. Eberhard, Design and calibration of zero-additional-phase SPIDER, J. Opt. Soc. B. **22**, 1875 (2005).

[15] M. Miranda, C. L. Arnold, T. Fordell, F. Silva, B. Alonso, R. Weigand, A. L'Huillier, and H. Crespo, Characterization of broadband few-cycle laser pulses with the d-scan technique, Opt. Express **20**, 18732 (2012).

[16] B. Rocio, O. Aurelio, B. Federico, De Silvestri. Sandro, C. Giulio, and M. Cristian, Optimized ancillae generation for ultra-broadband two-dimensional spectral-shearing interferometry, J. Opt. Soc. Am. B. **32**, 1851 (2015).

[17] E. Goulielmakis, M. Uiberacker, R. Kienberger, A. Baltuska, V. Yakovlev, A. Scrinzi, T. Westerwalbesloh, U. Kleineberg, U. Heinzmann, M. Drescher, and F. Krausz, Direct measurement of light waves, Science **305**, 1267 (2004).

[18] K. T. Kim, C. Zhang, A. D. Shiner, B. E. Schmidt, F. Légaré, D. Villeneuve, and P. Corkum, Petahertz optical oscilloscope, Nat. Photonics **7**, 958 (2013).

[19] A. S. Wyatt, T. Witting, A. Schiavi, D. Fabris, P. Matia-Hernando, I. A. Walmsley, J. P. Marangos, and J. W. Tisch, Attosecond sampling of arbitrary optical waveforms, Optica **3**, 303 (2016).

[20] Z. Yang, W. Cao, Y. Mo, H. Xu, K. Mi, P. Lan, Q. Zhang, and P. Lu, Alloptical attosecond time domain interferometry, Natl. Sci. Rev. **8**, nwaa211 (2021).

[21] Z. Yang, W. Cao, X. Chen, J. Zhang, Y. Mo, H. Xu, K. Mi, Q. Zhang, P. Lan, and P. Lu, All-optical frequency-resolved optical gating for isolated attosecond pulse reconstruction, Opt. Lett. **45**, 567 (2020).

[22] K. Mi, W. Cao, H. Xu, Y. Mo, Z. Yang, P. Lan, Q. Zhang, and P. Lu, Perturbed ac Stark Effect for Attosecond Optical-Waveform Sampling, Phys. Rev. Appl. **13**, 014032 (2020).

[23] D. J. Griffiths, *Introduction to Quantum Mechanics* (Cambridge: Pearson Prentice Hall, Upper Saddle River, 2005).

[24] See Supplemental Material at http://link.aps.org/supplemental/10.1103/PhysRevApplied.17.014046 for more details about the principle of the retrieval methods, retrieval results of complex pulses, retrieved optical waveforms using attosecond pulse train, and the polarization dependence of the transition amplitudes.

[25] M. B. Gaarde, C. Buth, J. L. Tate, and K. J. Schafer, Transient absorption and reshaping of ultrafast xuv light by laser-dressed helium, Phys. Rev. A **83**, 013419 (2011).

[26] M. Wu, S. Chen, M. B. Gaarde, and K. J. Schafer, Time-domain perspective on autler-townes splitting in attosecond transient absorption of laser-dressed helium atoms, Phys. Rev. A **88**, 043416 (2013).

[27] M. Wu, S. Chen, S. Camp, K. J. Schafer, and M. B. Gaarde, Theory of strong-field attosecond transient absorption, J. Phys. B: At. Mol. Opt. Phys. **49**, 062003 (2016).

[28] H. Xu, W. Cao, J. Zhang, Y. Mo, K. Mi, Z. Yang, Q. Zhang, and P. Lu, Mapping time-dependent quasi-energies of laser dressed helium, Opt. Express **29**, 11342 (2021).

[29] H. Paul, Interference and 'which way' information, Opt. Quantum Electron. **28**, 1111 (1996).

[30] A. Ten Wolde, L. Noordam, A. Lagendijk, and H. V. L. van Den Heuvell, Observation of Radially Localized Atomic Electron Wave Packets, Phys. Rev. Lett. **61**, 2099 (1988).

[31] J. A. Yeazell and C. Stroud Jr, Observation of Spatially Localized Atomic Electron Wave Packets, Phys. Rev. Lett. **60**, 1494 (1988).

[32] J. Mauritsson, T. Remetter, M. Swoboda, K. Klünder, A. L'Huillier, K. J. Schafer, O. Ghafur, F. Kelkensberg, W. Siu, P. Johnsson, M. J. J. Vrakking, I. Znakovskaya, T. Uphues, S. Zherebtsov, M. F. Kling, F. Lépine, E. Benedetti, F. Ferrari, G. Sansone, and M. Nisoli, Attosecond Electron Spectroscopy Using a Novel Interferometric Pump-Probe Technique, Phys. Rev. Lett. **105**, 053001 (2010).

[33] S. H. Autler and C. H. Townes, Stark effect in rapidly varying fields, Phys. Rev. **100**, 703 (1955).

[34] N. B. Delone and V. P. Krainov, Ac Stark shift of atomic energy levels, Physics-Uspekhi **42**, 669 (1999).

[35] M. Chini, B. Zhao, H. Wang, Y. Cheng, S. Hu, and Z. Chang, Subcycle ac Stark Shift of Helium Excited States Probed with Isolated Attosecond Pulses, Phys. Rev. Lett. **109**, 073601 (2012).

[36] S. Chen, M. J. Bell, A. R. Beck, H. Mashiko, M. Wu, A. N. Pfeiffer, M. B. Gaarde, D. M. Neumark, S. R. Leone, and K. J. Schafer, Light-induced states in attosecond transient absorption spectra of laser-dressed helium, Phys. Rev. A **86**, 063408 (2012).

[37] M. Chini, X. Wang, Y. Cheng, Y. Wu, D. Zhao, D. A. Telnov, S.-I. Chu, and Z. Chang, Sub-cycle oscillations in virtual states brought to light, Sci. Rep. **3**, 1 (2013).

[38] R. G. Brewer and R. Shoemaker, Optical free induction decay, Phys. Rev. A **6**, 2001 (1972).

[39] M. J. Bell, A. R. Beck, H. Mashiko, D. M. Neumark, and S. R. Leone, Intensity dependence of light-induced states in transient absorption of laser-dressed helium measured with isolated attosecond pulses, J. Mod. Opt. **60**, 1506 (2013).

[40] M. Reduzzi, J. Hummert, A. Dubrouil, F. Calegari, M. Nisoli, F. Frassetto, L. Poletto, S. Chen, M. Wu, M. B. Gaarde, K. Schafer, and G. Sansone, Polarization control

of absorption of virtual dressed states in helium, Phys. Rev. A **92**, 033408 (2015).

[41] A. R. Beck, D. M. Neumark, and S. R. Leone, Probing ultra-fast dynamics with attosecond transient absorption, Chem. Phys. Lett. **624**, 119 (2015).

[42] M. Kubullek, Z. Wang, K. von der Brelje, D. Zimin, P. Rosenberger, J. Schötz, M. Neuhaus, S. Sederberg, A. Staudte, N. Karpowicz, M. F. Kling, and B. Bergues, Single-shot carrier-envelope-phase measurement in ambient air, Optica **7**, 35 (2020).

[43] P. B. Corkum, Plasma Perspective on Strong Field Multiphoton Ionization, Phys. Rev. Lett. **71**, 1994 (1993).

[44] M. Lewenstein, P. Balcou, M. Y. Ivanov, A. L'huillier, and P. B. Corkum, Theory of high-harmonic generation by low-frequency laser fields, Phys. Rev. A **49**, 2117 (1994).